

Measurement of the Charge Collection Efficiency after Heavy Non-Uniform Irradiation in *BABAR* Silicon Detectors

S. Bettarini, M. Bondioli, L. Bosisio, G. Calderini, C. Campagnari, S. Dittongo, F. Forti, M. A. Giorgi, G. Marchiori*, G. Rizzo

Abstract—We have investigated the depletion voltage changes, the leakage current increase and the charge collection efficiency of a silicon microstrip detector identical to those used in the inner layers of the *BABAR* Silicon Vertex Tracker (SVT) after heavy non-uniform irradiation. A full SVT module with the front-end electronics connected has been irradiated with a 0.9 GeV electron beam up to a peak fluence of $3.5 \times 10^{14} e^-/\text{cm}^2$, well beyond the level causing substrate type inversion. We irradiated one of the two sensors composing the module with a non-uniform profile with $\sigma=1.4$ mm that simulates the conditions encountered in the *BABAR* experiment by the modules intersecting the horizontal machine plane. The position dependence of the charge collection properties and the depletion voltage have been investigated in detail using a 1060 nm LED and an innovative measuring technique based only on the digital output of the chip.

Index Terms—radiation damage, silicon detector

I. INTRODUCTION

SEVERAL tests have been made in the past to study the effects of radiation damage to the *BABAR* Silicon Vertex Tracker (SVT) sensors and to their front-end electronics, but the reduction of charge collection efficiency (CCE) after irradiation has never been measured quantitatively. In addition, it has never been directly demonstrated that a SVT module can be operated normally after substrate type-inversion. This is expected to happen at a dose of (3 ± 1) Mrad, based on measurements performed on test structures from the same wafers. To address these issues a module identical to those used in the inner layer of the SVT, with the front-end electronics connected, has been irradiated with a 0.9 GeV electron beam. A total peak fluence of $3.5 \times 10^{14} e^-/\text{cm}^2$, corresponding to a peak dose of 9.3 Mrad, has been delivered to the silicon. A second module, which has not been irradiated, has been used as a control sample to track variations in the environmental conditions.

II. RADIATION DAMAGE OF THE SVT

The *BABAR* experiment [1], at the SLAC PEP-II e^+e^- storage ring [2], has the primary physics goal of precisely measuring *CP*-violating asymmetries and rare branching fractions in

S. Bettarini, M. Bondioli, G. Calderini, F. Forti, M. A. Giorgi, G. Marchiori, G. Rizzo are with INFN-Pisa and Università degli studi di Pisa.

L. Bosisio and S. Dittongo are with INFN-Trieste and Università degli studi di Trieste.

C. Campagnari is with University of California at Santa Barbara.

M. A. Giorgi is also with Stanford Linear Accelerator Center.

*Corresponding author. *E-mail address:* giovanni.marchiori@pi.infn.it

B meson decays. $B\bar{B}$ pairs are produced in head-on collisions between 9.0 GeV electrons and 3.1 GeV positrons. Since a very large sample of *B* decays is needed, PEP-II was designed to deliver the high peak luminosity of $3 \times 10^{33} \text{cm}^{-2}\text{s}^{-1}$ (the production cross section is $\sigma_{e^+e^- \rightarrow B\bar{B}} = 1.1 \text{nb}$)

The Silicon Vertex Tracker [3] has been installed in *BABAR* in early 1999 and has been reliably operated for five years, providing excellent and efficient vertexing and tracking information. It is composed of five layers of 300 μm thick, double-sided microstrip detectors. p^+ strips on one side and n^+ strips on the other side, with orthogonal orientation with respect to the p^+ ones, are implanted on a high-resistivity n^- bulk. They are AC-coupled to the electronics via integrated decoupling capacitors. The detectors are operated in reverse mode at full depletion, with bias voltage V_{bias} typically 10V higher than the depletion voltage V_{depl} (which lies in the range 25V–35V). The leakage current under these conditions is lower than $15 \mu\text{A}$.

The main source of background in the SVT comes from showers originated in the material of the beam-pipe by off-momentum beam particles, which are over-bent by the permanent dipole magnets located in the proximity of the interaction point to separate the two beams. The dose absorbed by the silicon, which is measured by means of 12 silicon p-i-n diodes close to the inner layer of the SVT, varies strongly as a function of the azimuthal angle around the beamline, and is highly peaked in a narrow region of the (horizontal) bend plane of the machine, following a roughly gaussian distribution with $\sigma \approx 2$ mm.

The inner layer of the SVT, located at a radius of 3.3 cm from the beam line, receives the highest dose. At design luminosity the average dose for the silicon of the inner layer was expected to be 33 krad/yr, peaking to 240 krad/yr in the horizontal region. The detectors were therefore originally designed to withstand up to 2 Mrad of total radiation dose, which would have been reached, in ten years of running, only in the inner horizontal region of the SVT, and which is expected to be less than the dose at which bulk type-inversion occurs. However, PEP-II excellent performance has been significantly higher than expected. The peak instantaneous luminosity has reached $9 \times 10^{33} \text{cm}^{-2}\text{s}^{-1}$, three times the design value, and is expected to increase up to $2 \times 10^{34} \text{cm}^{-2}\text{s}^{-1}$. A thin horizontal region of the inner part of the detector has thus already received the dose budget of 2 Mrad and will receive 9 Mrad by 2009,

whereas a larger fraction of silicon in the inner layers away from the horizontal plane should accumulate a dose between 2 and 5 Mrad by the same date.

III. PRINCIPLE OF THE CCE MEASUREMENT

The basic idea of the measurement is to use a 1060 nm LED, whose attenuation length $\lambda_{\text{att}} = 1$ mm is deeper than the 300 μm of the silicon thickness, to generate charges in the sensors. The charges then drift in the fully depleted silicon and the signals induced on the microstrip electrodes on the two sides of the detectors and amplified by the front-end electronics.

Each readout strip of the sensors, whose pitch is 50 μm on the n-side and 100 μm on the p-side, is connected to one of the 128 channels of the AToM IC [4]. The AToM IC is a custom readout chip produced with a Honeywell rad-hard 0.8 μm CMOS process. It is capable of simultaneous acquisition, digitization and readout. Each channel of the AToM IC, as shown in Figure 1, has an analog section consisting of a low-noise charge-sensitive pre-amplifier followed by a CR-(RC)² shaper, whose output is coupled differentially into a comparator. The nominal gain of the pre-amplifier is 250 mV/fC. The shaping time is programmable, with a minimum of 100 ns, up to 400 ns. In our measurements we used the 100 ns setting, which is also used in the modules in the inner layers of the SVT. The comparator threshold is controlled by an on-chip 6-bit DAC (Thresh DAC) whose least significant bit (LSB) has a nominal value of 12.5 mV, corresponding to a charge of 0.05 fC at the pre-amplifier's input. The comparator output goes to an SRAM pipeline, which provides a trigger latency of 12.93 μs . When the input to the comparator exceeds the pre-set threshold, the output goes high and a series of ones is clocked into the pipeline. A calibration charge can be injected into the preamplifier by means of a 50 fF capacitor (C_{inj}) connected with a switch to the pre-amplifier input and controlled by a 6-bit DAC (CAL DAC). The CAL DAC LSB has a nominal value of 10 mV, corresponding to a charge on the C_{inj} capacitor of 0.5 fC.

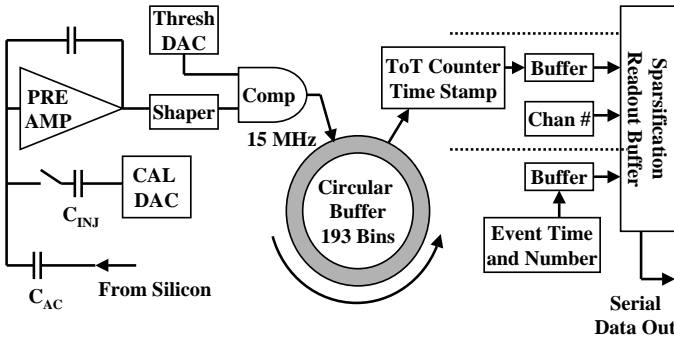


Fig. 1. Schematic diagram of the AToM front-end IC.

Upon receipt of an external trigger, a selectable region in the pipeline is searched for a zero-to-one transition. The transition

indicates a “hit” and the number of following ones at the comparator output, divided by the clock period, represents the time-over-threshold (TOT) of the hit, which is stored as a 4-bit number and has an approximately logarithmic dependence on the input charge. This allows charge measurement over a broad dynamic range (≈ 40 fC) with a limited number of bits, but the limited accuracy makes the TOT unsuitable for the purpose of our measurement, where a good analog resolution is needed in order to establish small drops in the CCE. Therefore we have turned to an alternative method of measuring the charge, based on “threshold scans” [5].

A threshold scan consists in measuring, for each read-out channel i at fixed injected charge Q_i at the input of the pre-amplifier, the hit efficiency as a function of the pre-set threshold of the comparator, which is varied inside the full dynamic range. Q_i can be either a calibration charge injected through the calibration capacitor, or the charge induced in read-out channel i by the charge generated in the silicon by the LED. The 50% turning point of the hit efficiency versus threshold distribution is the threshold offset $V_{\text{off}}(i, Q_i)$ for the channel i at charge Q_i , as shown in Figure 2. The threshold offset has a linear dependence

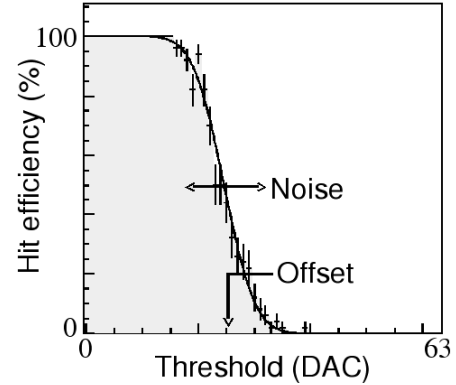


Fig. 2. Schematic representation of a threshold scan for a single readout channel.

on the charge which is given by the following expression:

$$V_{\text{off}}(i, Q_i) = P_i + Q_i \times G_i \quad (1)$$

The pedestal $P_i \equiv V_{\text{off}}(i, Q_i = 0)$ and the gain $G_i \equiv dV_{\text{off}}(i, Q_i)/dQ_i$ of the i -th electronic channel can be accurately determined by performing threshold scans with different calibration charges and fitting the V_{off} vs Q_i distribution with a linear function.

When the LED is used to generate charge in the silicon, the charge at the input of the pre-amplifier of the i -th channel is $Q_i = Q_{\text{LED}} \times f(i) \times \text{CCE}_i$, where Q_{LED} is the total charge release by the LED in the silicon, which is proportional to the LED intensity, CCE_i is the local charge collection efficiency of the silicon and $f(i)$ accounts for division of the charge between the channels and the angular distribution of the LED power. When the detector is fully depleted and the electric

field intensity is sufficient to collect almost all the charge, $\Sigma_i f(i) = 1$ (for both sides) and the CCE as a function of the reverse bias voltage applied to the silicon saturates. In our case the LED is current-driven and the light flux is proportional to the LED current, therefore $Q_{LED} = a \times I_{LED}$. In a threshold scan performed with the silicon illuminated by the LED with current I_{LED} therefore the offset of the i -th channel is given by

$$V_{off}(i, I_{LED}) = P_i + a \times I_{LED} \times f(i) \times CCE_i \times G_i \quad (2)$$

From threshold scans at different values of the LED current one can extract for each channel, by performing a linear fit to the $V_{off}(i, I_{LED})$ vs I_{LED} distribution, the slope $S_i \equiv a \times f(i) \times G_i \times CCE_i$. By dividing the slope S_i for the electronics gain G_i and summing over all channels we obtain therefore a quantity which is proportional to the average CCE in the silicon region illuminated by the LED:

$$a \times \langle CCE \rangle = \Sigma_i S_i / G_i \quad (3)$$

By comparing the sum $\Sigma_i S_i / G_i$ before and after the irradiation of the detectors we can therefore monitor the relative CCE drop.

IV. EXPERIMENTAL SETUP

A. Setup for the CCE measurement

The LED is a current-driven EG&G C30116 model, with peak wavelength $\lambda_{peak} = 1060$ nm, risetime $t_{rise} < 10$ ns, typical peak flux vs LED current $\phi_{peak}/I_{LED} = 2$ mW/A. It is connected through a 1 k Ω resistor to a GPIB-controlled pulser. A thin brass foil with a 500 μ m diameter pinhole in it is placed at a distance of 3 mm from the LED lens surface. A converging lens with focal length $f = 45$ mm is placed at a distance of 90 mm from the pinhole and at the same distance from the module plane, thus ensuring that the pinhole image is focused in the module plane. In our measurements the light emitted from the LED enters the silicon from the n^+ -doped (ohmic) side. The dimension of the luminous spot has been chosen to be narrower than the region in which the CCE, after irradiation with a beam with $\sigma \approx 2$ mm, is supposed to change, but at the same time it is large enough that the uncertainty in the relative alignment of the LED and the silicon detectors (< 100 μ m) has a negligible impact on the uncertainty on the measured CCE. The LED, the pinhole and the lens are mounted inside a brass cylinder attached to a mechanical arm of a GPIB-controlled X-Y stage. A picture of the mechanical setup is shown in Figure 3.

The charge generated in the silicon is controlled by changing the amplitude of the pulse driving the LED. We have selected a range of amplitudes in which the LED response is linear and the signal at the shaper output remains within the limited dynamic range of the THR-DAC, as shown in Figure 4.

The measurement process is fully automated: a workstation controls via GPIB connections the motion of the X-Y stage and the voltage setting of the pulser, while at the same time controls through an ethernet interface a VME-based computer which is responsible for sending trigger signals to the pulser

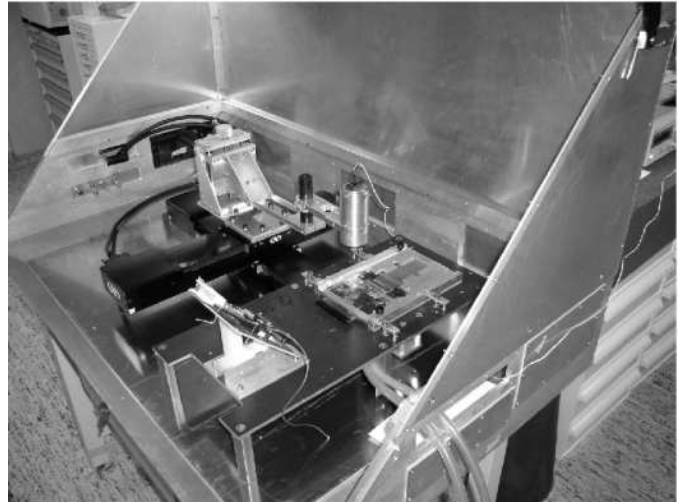


Fig. 3. Mechanical setup for the CCE measurements. The silicon module is mounted in a metal frame, and above it the brass cylinder holding the LED is clearly visible. The LED is moved above the detector surface by means of the black X-Y stage.

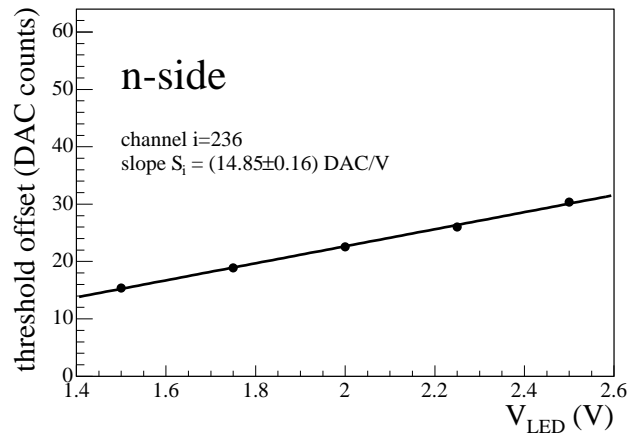


Fig. 4. Distribution, for one readout channel illuminated by the LED, of the threshold offset V_{off} (the 50% hit efficiency turn-on point) as a function of the amplitude of the pulse driving the LED (dots). The result of a linear fit to this distribution is superimposed (solid line).

and to the readout section of the front end electronics. An example of the distribution of S_i/G_i vs channel measured with this setup is shown in Figure 5: the peak width is fully consistent with the pinhole size and the readout pitch of the strips. Once the S_i/G_i distribution has been measured, an offline algorithm identifies the position of the peak, evaluates the baseline in channels away from the peak, and computes the baseline-subtracted sum $\Sigma_i S_i / G_i$ over the whole peak, which is proportional to the average CCE in the point illuminated by the LED. Repeated tests on the control module have shown that the single measurement resolution is about 2%. Alignment in the relative position between the module and the X-Y stage and aplanarity effects have been found to introduce negligible degradation in the CCE resolution. Moreover, no significant

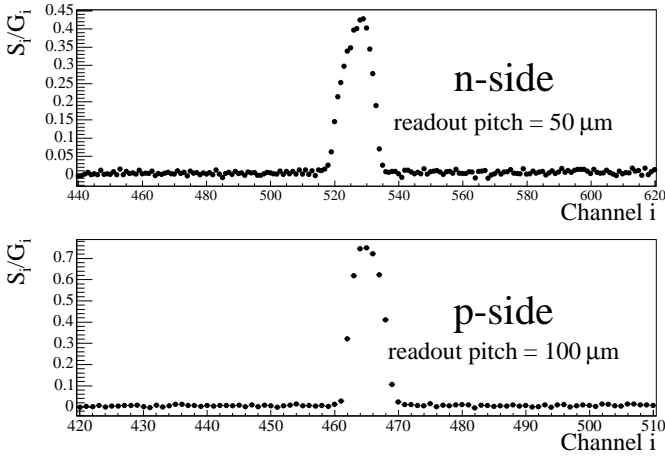


Fig. 5. Distribution of the fitted slopes S_i divided by the electronic gain G_i as a function of the readout channel i . A peak in the channels illuminated by the LED is clearly visible. The integral of the peak is proportional to the average charge collection efficiency in the illuminated area.

variation (compared to the 2% intrinsic resolution) of the measured CCE has been observed over a period of several hours of continuous operations. However, differences up to 10% have been found in CCE measurements performed in different runs. For this reason the CCE measured for the irradiated module has always been normalized to the average CCE measured, with a high number of samplings, in a fixed set of points of the control module in the same environmental conditions.

B. Setup for the silicon irradiation

The module irradiation has been performed at the Elettra Synchrotron facility in Trieste with a 0.9 GeV electron beam. The irradiation has been performed in six steps reaching a total peak dose of about 9 Mrad. During each irradiation step the module is mounted on a X-Y stage, which is located at the end of the Linac and is remotely controlled from the Linac Control Room through a serial connection. Prior to the irradiation a radiochromic dosimetry film is placed close to the surface of the silicon, to keep trace of the beam position during the irradiation. Another radiochromic film is placed above the chip region to check that the electronics does not receive a significant dose, thus avoiding the need in the CCE measurement to disentangle effects caused by radiation damage to the silicon from effects caused by damage to the electronics. A third radiochromic film is attached to the edge of the metal frame which hosts the module and is irradiated for a few seconds (to avoid saturation) to obtain an image of the beam profile, which is necessary to estimate the beam size and is used to perform the alignment between the module and the beam. The beam spot obtained with this method is shown in Figure 6. Two sets of test structures from the same wafer as the silicon detectors are mounted on the module frame in a position which corresponds to the center of the zone to be irradiated. Two pictures of the module setup are shown in Figures 7 and 8.

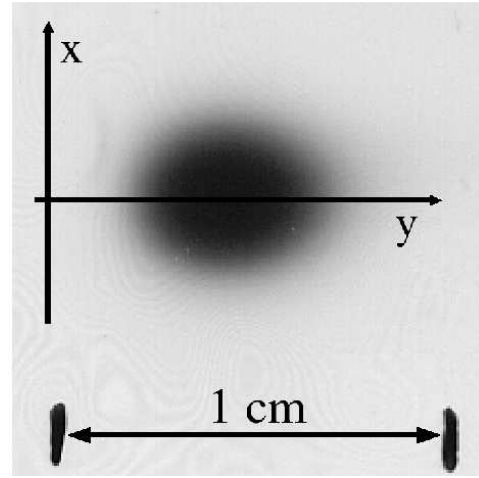


Fig. 6. Beam spot obtained on a radiochromic dosimetry film irradiated for a few seconds.

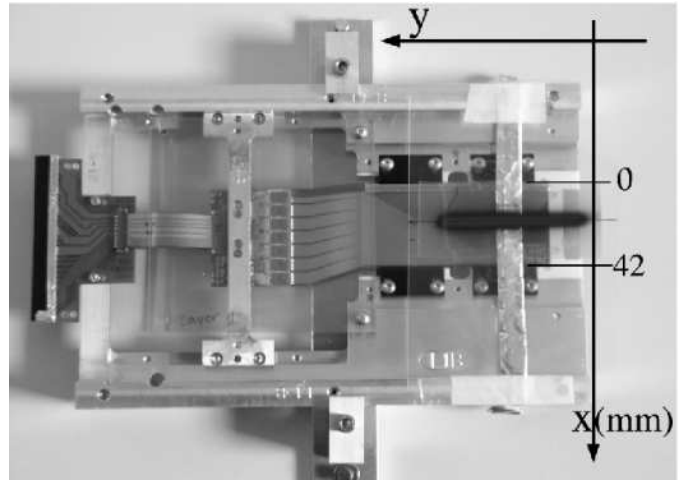


Fig. 7. Picture of the irradiated module. During the irradiation the beam comes from the side not shown here. The radiochromic film keeps trace (dark stripe at $x \approx 21$ mm) of the beam position. The aluminum foil contains test structures used as a cross-check for the dose evaluation as described in the text.

After alignment of the module with respect to the beamline, the linac is turned on and the module is moved back and forth several times along a line in a plane perpendicular to the beam. The detector is 82 mm long in the direction (y) of the irradiation and 42 mm wide in the direction (x) orthogonal to the irradiation. The beam has a gaussian profile whose width along the x axis, accurately measured by digitizing and analyzing the spot obtained on the radiochromic dosimetry film irradiated for a few seconds, is $\sigma_x \approx 1.4$ mm. By moving the module with constant velocity $v_y = 1$ mm/s a 50 mm long region of the silicon is irradiated, with a dose profile which is uniform in y and gaussian in x , centered on the axis of the module and with width equal to the beam width σ_x . The beam remains several centimeters far from the chips during all the irradiation.



Fig. 8. Mechanical setup of the module for the irradiation. The module (at the center) is mounted on a X-Y stage (bottom) in proximity of the end-flange of the Elettra linac.

The peak fluence ϕ_e and hence the peak dose are determined from the beam spread, the speed at which the module is moved during the irradiation, the number of times N_{sweeps} this operation is performed and the linac current I_{linac} through the relation $\phi_e = N_{\text{sweeps}}(I_{\text{linac}}/q)/(\sqrt{2\pi}v_y\sigma_x)$ where $q = 1.6 \times 10^{-19}\text{C}$ is the electron charge. For typical values ($\sigma_x = 1.4$ mm, $v_y = 1$ mm/s, $I_{\text{linac}} = 30$ nA and $N_{\text{sweeps}} = 10$), a total peak fluence of about $5.3 \times 10^{13} e^-/\text{cm}^2$ (corresponding to a peak dose of about 1.4 Mrad) is delivered to the module in about ten minutes. The linac current is measured with 4% accuracy from the current flowing in a toroidal coil coaxial with the beam and is the dominating source of uncertainty in the peak fluence estimate. A less precise dose estimate, obtained from the increase in leakage current in the test structures irradiated with the detector, is used as a cross check and is consistent with the estimate from the linac current.

V. RESULTS

A. Leakage current increase

After each irradiation step we have measured the leakage current of the module from standard I-V curves at reverse bias. The leakage current increases linearly with the accumulated dose of the whole module, as shown in Figure 9. The current increase vs dose per unit area is $(2.1 \pm 0.1)\mu\text{A}/\text{cm}^2/\text{Mrad}$, normalized at a temperature of 23°C , consistent with the increase observed in the SVT during BABAR operation. The damage constant $\alpha \equiv \Delta J_{\text{leak}}/\langle\phi_e\rangle$, where J_{leak} is the leakage current density and $\langle\phi_e\rangle$ is the average electron fluence delivered to the silicon, is $\alpha = (1.37 \pm 0.07)10^{-18}$ A/cm, normalized at 20°C .

B. Depletion voltage shift

After each irradiation we have measured, in a point at the center of the most irradiated zone of the detector, the sum

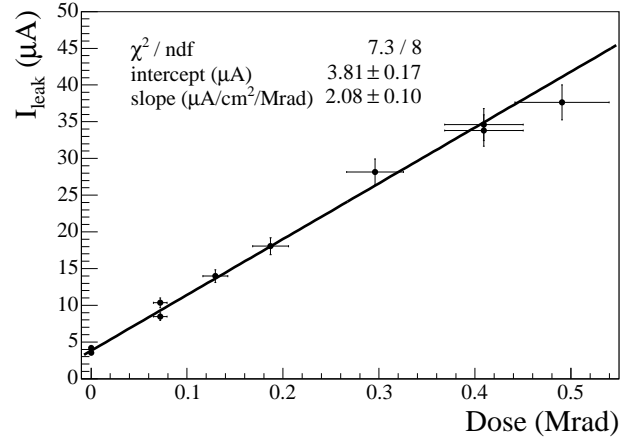


Fig. 9. Leakage current increase after irradiation. The silicon area is 42.4×82.6 mm².

$\sum_i S_i/G_i$ (which is proportional to the local CCE) as a function of the reverse bias voltage V_{bias} applied to the silicon. This is shown, up to the fifth irradiation step, in Figure 10.

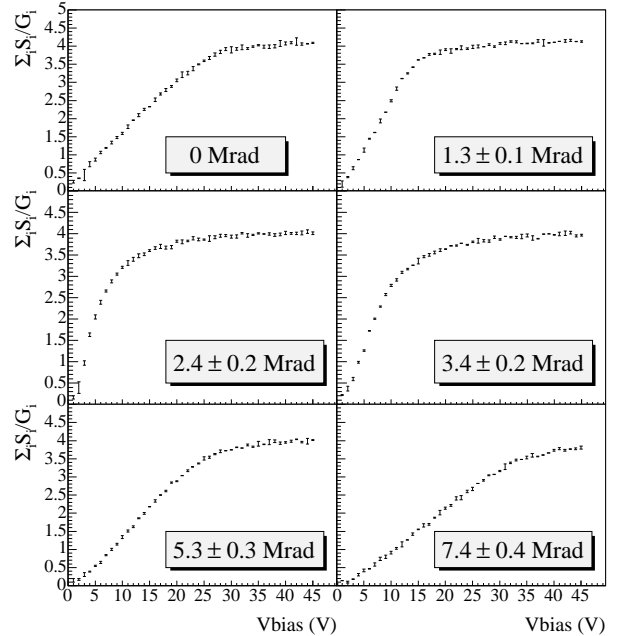


Fig. 10. Measured $\sum_i S_i/G_i$ as a function of bias voltage, for the same point of the silicon and six different integrated doses. The plotted quantity is proportional to the charge collection efficiency of the silicon.

We use the voltage value V_{sat} at which the sum $\sum_i S_i/G_i$ and therefore the CCE saturate as an estimator for the depletion voltage V_{depl} of the silicon in the point illuminated by the LED. This is not a good estimator when V_{depl} is close to 0V, because in that case there is a bias voltage range in which the detector is fully depleted but the electric field inside it is not intense enough to achieve signal saturation. Indeed, we see that the

CCE never saturates at bias voltages lower than about 10V. However, when the depletion voltage is higher than 10V then V_{sat} is a good estimator for V_{depl} : for instance, prior to the first irradiation step we estimate $V_{\text{sat}} \approx (31 \pm 1)\text{V}$, which is consistent with the depletion voltage $V_{\text{depl}} = 25\text{V}$ measured in structure tests from the same wafer. As shown in Figure 10, the depletion voltage in the damaged silicon first decreases with dose, than starts to increase again. The inversion occurs at (2.4 ± 1.0) Mrad and corresponds to the bulk type inversion of the silicon. After type inversion the detector continues to operate without any problem.

To confirm that V_{sat} is a good estimator of the depletion voltage, which is shifted by bulk damage of the silicon, we measure - after the second irradiation step, corresponding to a total peak dose of 2.5 Mrad - V_{sat} in a set of 21 points, equally spaced (at 1mm steps), on a line which is orthogonal to the irradiation direction and crosses the irradiated region. The distribution of V_{sat} , shown in Figure 11, exhibits a clear peak whose width is consistent with the measured beam spread.

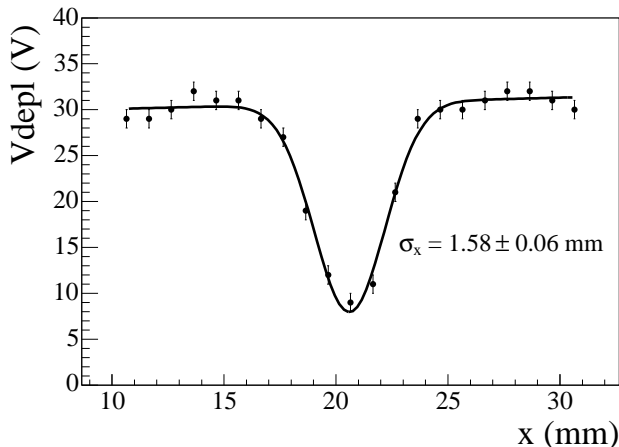


Fig. 11. Depletion voltage as a function of the position, after two irradiation steps (total peak dose ≈ 2.5 Mrad at $x=20.5$ mm), for a set of points on a line orthogonal to the irradiation direction.

C. Charge collection efficiency drop

The CCE has been measured, before and after irradiation, in a grid of 30×30 points spanning almost all the surface of the irradiated module. The ratio between the CCE measured after the last irradiation step and the CCE before irradiation, for the p-side, is shown in Figure 12.

In Figure 13 we compare the CCE drop in points at the center of the irradiated zone (the darker central rectangle in Figure 12), which have received a total dose of (8.5 ± 0.8) Mrad, with points which are at least 4σ away from the irradiation axis and have received a dose of only a few krad (the lighter lateral rectangles in Figure 12). For points in the irradiated zone we measure a CCE decrease equal to $(6 \pm 2)\%$ on the p-side and $(9 \pm 2)\%$ on the n-side, while no CCE decrease is observed for points which have received a negligible dose.

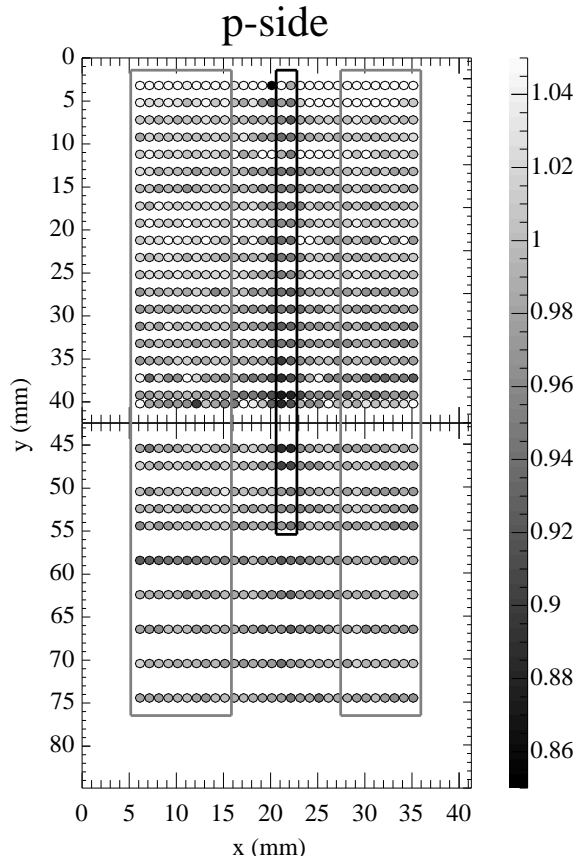


Fig. 12. Ratio between the CCE after and before irradiation, as a function of the position on the module. Only the p-side is shown. The two squares surrounded by tick marks represent the two silicon detectors that compose the module. The darker central rectangle surrounds the most irradiated region (the average dose in the points enclosed by the rectangle is (8.5 ± 0.8) Mrad). The points inside the lateral, lighter rectangles are at least 4σ away from the beam axis and have received a negligible dose.

VI. CONCLUSION

We have irradiated, with a 0.9 GeV e^- beam, a silicon detector identical to those in the BABAR Silicon Vertex Tracker. We have implemented a fully automated setup by means of which we can generate charge in the silicon through illumination with a 1060 nm LED and measure the charge collection efficiency through an innovative method based on the digital output of the front-end electronics connected to the detector. We have measured an increase in leakage current at 23°C of $(2.1 \pm 0.1)\mu\text{A}/\text{cm}^2/\text{Mrad}$. The detector, whose initial depletion voltage was 25V, has undergone type inversion at a dose of (2.4 ± 1.0) Mrad, after which it has continued to operate without any problem. We have measured, in points irradiated with a dose of (8.5 ± 0.8) Mrad, a moderate charge collection efficiency decrease equal to $(6 \pm 2)\%$ on the p-side and $(9 \pm 2)\%$ on the n-side. We have thus demonstrated that the SVT sensors can be operated for the whole lifetime of the BABAR experiment and that bulk damage in the silicon will cause only a modest

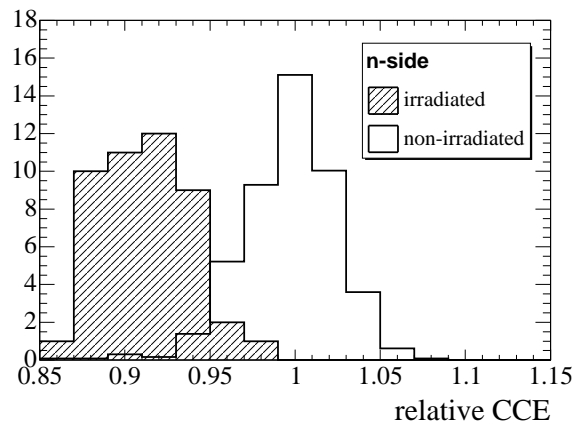
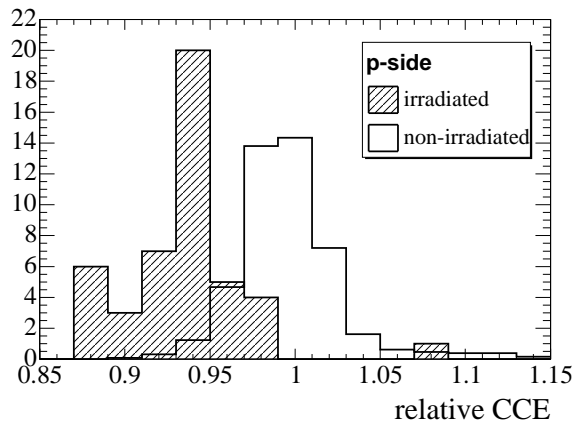


Fig. 13. Ratio between the CCE after and before irradiation, for points which have received a dose of (8.5 ± 0.8) Mrad (hatched histograms) and points which have received a negligible dose (hollow histograms). Top: p-side. Bottom: n-side.

impact on their performances.

REFERENCES

- [1] *BABAR* Collaboration, B. Aubert et al., "The BaBar detector" *Nucl. Instrum. Meth.* vol. A479, pp. 1-116, 2002.
- [2] "PEP-II – An asymmetric *B* Factory, Conceptual Design Report", SLAC-418, LBL-5379, 1993.
- [3] D. Barbieri et al., "Silicon sensors for the *BABAR* Vertex Tracker: Design, Electrical Tests and Production Quality Control", *Nuovo Cimento*, vol. A112, pp.113-130, 1999.
- [4] V. Re et al, "The Rad-Hard Readout System of the *BABAR* Silicon Vertex Tracker", *Nucl. Instrum. Meth.* vol. A409, pp. 354-359, 1998.
- [5] C. Campagnari et al (1998, August). Study of SVT gains. [Online]. Available: <http://charm.physics.ucsb.edu/BaBar/LedGainStudy.html>